




## Article

# Differentiation in the SiC Filler Size Effect in the Mechanical and Tribological Properties of Friction-Spot-Welded AA5083-H116 Alloy

S. Suresh <sup>1,\*</sup> , Elango Natarajan <sup>2,3,\*</sup> , Gérald Franz <sup>4,\*</sup>  and S. Rajesh <sup>5</sup>

<sup>1</sup> Department of Mechanical Engineering, Muthayammal Engineering College, Rasipuram 637408, Tamil Nadu, India

<sup>2</sup> Faculty of Engineering, Technology and Built Environment, UCSI University, Kuala Lumpur 56000, Malaysia

<sup>3</sup> Department of Mechanical Engineering, PSG Institute of Technology and Applied Research, Coimbatore 641062, Tamil Nadu, India

<sup>4</sup> Laboratoire des Technologies Innovantes, UR UPJV 3899, Avenue des Facultés, Le Bailly, 80025 Amiens, France

<sup>5</sup> Department of Mechanical Engineering, Knowledge Institute of Technology, Salem 637504, Tamil Nadu, India

\* Correspondence: suresh.mjl@gmail.com (S.S.); elango@ucsiuniversity.edu.my (E.N.); gerald.franz@u-picardie.fr (G.F.)

**Abstract:** Ceramic reinforced friction stir spot-welding (FSSW) is one of the unique welding techniques used to fabricate spot joints. This study is intended to investigate the effect of reinforcement additive particle size in achieving higher weld strengths. AA5083-H116 aluminum alloy plates were welded with nano- and micro-sized silicon carbide (SiC) particles. Investigations of the weld joints prepared using a tool rotational speed of 1300 rpm, tool plunge rate of 25 mm/min, and dwell time of 10 s revealed that the lap shear tensile strength and hardness of the nano-SiC particles added to aluminum joints were higher than those of the micro-SiC particles added to joints. In particular, the nano-SiC particles provided 29.6% higher strength and 23.3% higher hardness than the unfilled FSSW. The uniformly dispersed fine SiC particles in the processed zone provided more nucleation sites for the re-precipitation of new grains and the precipitates in the aluminum matrix. The X-ray diffraction results confirmed that there was no evidence of a new phase (intermetallic compounds). Reinforcement of SiC particles significantly enhanced the wear characteristics, as well (26.3%). Field emission scanning electron microscopy (FESEM) evidenced the uniform distribution of SiC particles in the weld nugget zone. In addition, the fractography of the samples is presented and discussed.

**Keywords:** FSSW; AA5083-H116 aluminum alloy; silicon carbide; lap shear strength; microhardness



**Citation:** Suresh, S.; Natarajan, E.; Franz, G.; Rajesh, S. Differentiation in the SiC Filler Size Effect in the Mechanical and Tribological Properties of Friction-Spot-Welded AA5083-H116 Alloy. *Fibers* **2022**, *10*, 109. <https://doi.org/10.3390/fib10120109>

Academic Editor: Lucian Blaga

Received: 29 October 2022

Accepted: 13 December 2022

Published: 15 December 2022

**Publisher's Note:** MDPI stays neutral with regard to jurisdictional claims in published maps and institutional affiliations.



**Copyright:** © 2022 by the authors. Licensee MDPI, Basel, Switzerland. This article is an open access article distributed under the terms and conditions of the Creative Commons Attribution (CC BY) license (<https://creativecommons.org/licenses/by/4.0/>).

## 1. Introduction

AA5083-H116 is a non-heat-treatable Al-Mg alloy. It finds applications in automobile/aircraft structures, pressure vessels, gas/oil piping, and cryogenics due to its excellent corrosion resistance and moderate strength [1]. The excellent mechanical and tribological properties of aluminum-based metal matrix composites make them a better replacement for commercially used aluminum alloy [2,3]. AA5083 contains 4% to 4.5% of Mg that can be subjected to stress corrosion cracking if it is exposed to service temperatures for long periods of time [4]. Achieving high-quality welds using Al-Mg alloys via the conventional spot-welding process and fusion welding is risky because of the high heat energy input and vaporization of the alloying elements [5].

Friction stir spot-welding (FSSW) is a new technology that is being utilized by companies such as Mazda Motors to produce spot joints in various places for welding aluminum. In FSSW, a non-consumable tool is rotated and pressed with a high force against the top surface of two overlapping sheets. The frictional heat and the applied pressure bond the components metallurgically, without melting. The tool is drawn out of the workpiece

after a dwell time. This solid-state welding process overcomes the difficulties in the conventional joining process and eliminates the issues such as electrode wear and tool life that resistance spot welding carried [6,7]. As automotive manufactures extend the utilization of lightweight materials, such as aluminum, magnesium, and other high-strength, lightweight combinations, interest in elective joining technologies is expanded. In FSSW, a non-consumable hardened rotating tool is plunged into the over lapped sheets, held for a short period time, and then retracted to produce a spot joint. The friction between the workpiece with the tool pin and the shoulder provides adequate heating and intermixing of the materials to produce a joint [8]. The aerospace and rail industries have recently expressed interest in FSSW, and there is an extended breadth of interest in the automotive industry, as well [6,9].

Numerous studies about the optimization of FSSW parameters (tool rotational speed, tool plunge depth, and dwell time) have been published, and different tool configurations result in high weld quality in dissimilar welding and similar welding techniques, as well [10,11]. Bagheri et al. [12] utilized mechanical vibration to join AA5058 sheets using FSSW and named it friction stir spot-vibration-welding (FSSVW). They reported that the FSSW joint efficiency was increased if vibration was applied in the range of 28 Hz to 38 Hz during FSSVW. Kalaf et al. [13] fabricated AA5052 composite joints using the FSSW process with a carbon-fiber-reinforced polymer as the interlayer, and they reported that the presence of intermetallic compounds (Al-Mg-C) enhanced the intermetallic bonding between the elements. They also reported that the interlayer addition decreased the tensile shear load through the formation of micro-cracks within the stir zone. Table 1 shows the research works concerning the FSSW of Al alloys in recent years.

**Table 1.** Recently published literature on the FSSW of aluminum alloys.

Reference	Description	Significance/Findings of the Research
Bagheri et al., 2022 [14]	Al/Cu composite FSSW joints with the addition of SiC particles	Homogeneous distribution of a finer, nanoparticle-sized SiC additive particles in the matrix causes higher shear tensile and Von-Mises stress.
Akinlabi et al., 2022 [15]	AA5083-H116 FSSW joint	Process parameters such as tool rotational speed and dwell time play a significant role in the improvement of structural, mechanical, and corrosion properties.
Hassanifard et al., 2022 [16]	7075-T6 joints through the inclusion of Al <sub>2</sub> O <sub>3</sub> particles	The addition of Al <sub>2</sub> O <sub>3</sub> nano-sized particles progress the improvement of the fatigue performance of the joint due to grain refinement.
Janga and Awang, 2022 [17]	Refill FSSW of thin AA7075-T6 sheets	Weld zone temperature and strain rate increase with an increase in tool shoulder plunge depth.
Tiwan et al., 2022 [18]	AA2024-O FSSW joints with variable tool pin configurations	The result showed that the maximum shear stress produced with the cylindrical pin FSSW tool was due to better material flow behavior during the process.
Karthikeyan, 2021 [19]	FSSW of AA6061, AA2024, and AA7075	Lower tool rotational speed and lower plunge rate are found to be optimum to friction stir spot-weld high-strength aluminum alloys compared to low-strength aluminum alloys.
Balamurugan and Mohan, 2021 [20]	FSSW of AA5052 and AA6061 with various tool pin profiles	Tool pin profile (pin diameter, length, and taper angle) strongly influences the refined and uniformly distributed grain structure.
Gao et al., 2020 [21]	Pre-hole FSSW of AA2219 to AA3003	The PFSSW method has a significant impact on the mechanical properties of the joint and weld microstructures due to the fascinating mixing features and solid metallurgical bonds between the base alloys.
Suryanarayanan and Sridhar, 2020 [22]	Pin-less FSSW of Al 5754-Al 6061	FSSW with a pin-less tool overcomes the drawbacks of the stress concentration factor and corrosion.

Table 1. Cont.

Reference	Description	Significance/Findings of the Research
Rohani Yazdi et al., 2019 [23]	FSSW of AA 6061-T6 with pin-less tool	Higher plunge depth of tool shoulder improves the volume of the displaced metal, resulting in high joint strength.
Suresh et al., 2019 [24]	AA6061-T6 swept FSSW joint	Additional stirring action of the tool causes the joints to become stronger than conventional FSSW joints.
Fahmy et al., 2018 [25]	RSW and FSSW of AA2024-T3	FSSW produces welds with finer grain structures than welds produced by RSW due to the crushing, stirring, and forging action of the welding tool.
Sun et al., 2018 [26]	Low-temperature FSSW of AA6061-T6	Low rotational speed leads to higher lap shear strength.

The reinforcement of particles in metallic materials to enhance the properties of the base metal has gained attention in various sectors such as the automobile, marine, and aerospace industries [27]. The use of various reinforcement particles (SiC, B<sub>4</sub>C, TiC, Y<sub>2</sub>O<sub>3</sub>, TiB<sub>2</sub>, Al<sub>2</sub>O<sub>3</sub>, and ZrB<sub>2</sub>) has been attempted in the friction stir welding (FSW) of aluminum matrix composite joints [28–30]. In recent years, FSSW has attempted to join metal sheets with filler particles (secondary particles) in the weld region to enhance the resulting weld properties [31–34]. Wu et al. [32] performed FSSW on an AZ31 magnesium alloy with SiC and found strengthened grain boundaries and increased mechanical properties. Tebyani et al. [33] employed nano-SiC (25 nm) to fabricate an interstitial-free steel FSSW joint, and they claimed that the hardness and joint strength were greatly enhanced compared to particle-free FSSW joints. Suresh et al. [34] investigated the optimum volume of nano-SiC particles and their effect on the mechanical properties of AA6061-T6 aluminum alloy FSSW joints. Substantial research findings are available on the FSSW of aluminum alloys, but no study has reported on the mechanical properties of AA5083-H116 friction stir spot-welds with the addition of ceramic particles. Further, the influence of ceramic particle size on the weld strength of FSSW joints has not yet been addressed.

The aim of the current research is to convene AA5083/SiC composite FSSW joints and investigate the effect of micro- and nano-fillers on their mechanical properties, wear properties, and microstructures. To this end, this paper is organized as follows: the materials and experimental methods are presented in Section 2, while Section 3 discusses the results and the research findings.

## 2. Materials and Methods

A 2-mm-thick commercial AA5083 aluminum alloy in an initial temper condition of H116 was used as the base metal. The chemical composition of the base metal (%) was 4.0–4.5 Mg, 1.2 Si, 0.4–1.0 Mn, 0.4 Fe, 0.4 Si, 0.25 Zn, 0.15 Cr, 0.1 Cu, and 0.05–0.25 Cr, with the remainder comprised of Al. The base material was sized to 100 mm × 35 mm by using wire-cut electrical discharge machining (EDM). The SiC particles, with mean sizes of 2 μm and 50 nm, were purchased from HONGWU International Group LTD (Guangzhou, China) and used as reinforcements in the friction-stirred area. Figure 1 shows the FESEM of the received particles.

The FSSW experiments were performed in a CNC vertical machining center. The sequence of the steps in the weld process are depicted in Figure 2. The guide hole was prepared on weld coupons to pack the SiC particles. The top and bottom plates were overlapped by 35 mm and the particles were packed tightly in the guide hole before the welding was completed. The schematic of the position of the guide hole and the welded joint portion is shown in Figure 2, sections A-A and X-X, respectively. Prior to beginning to weld, the specimens were first fixed into the custom fixture, as shown in Figure 3a. The CNC vertical machining center and the fixture created to clamp the specimens are shown in Figure 3a. The FSSW tool used for the welding process was made of H13 tool steel, with a hardness of 52–56 HRC (Figure 3b). The characteristics of the FSSW tool are listed in Table 2. The hole in the center of overlapped area was filled with micro-SiC particles

(2  $\mu\text{m}$  in size). Based on the trial experiments and the published literature [35–37], the tool rotational speed, tool plunge rate, and dwell time were fixed at 1300 rpm, 25 mm/min, and 10 s, respectively. Three samples in each condition were prepared for the investigation and analysis. Figure 3c shows the FSSW jointed samples. The same procedures and welding conditions were followed for preparing the nano-SiC particle (50 nm)-reinforced FSSW composite joints.

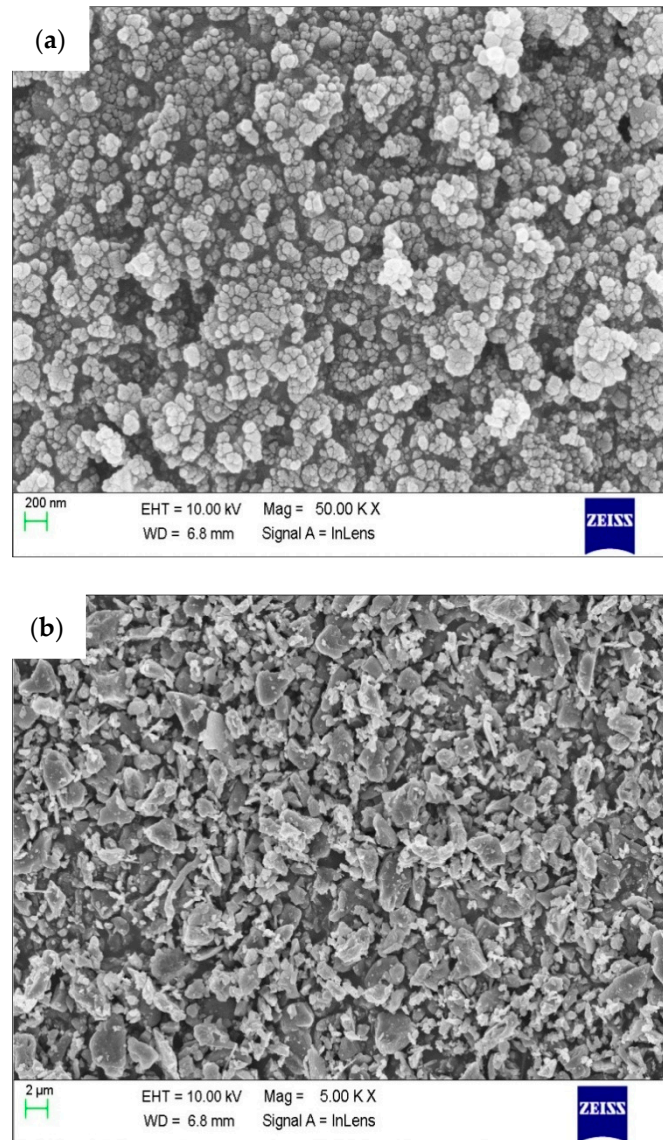


**Figure 1.** FESEM image of the as-received particles: (a) nano-SiC, and (b) micro-SiC.

**Table 2.** Characteristics of the FSSW tool.

Material	Pin Diameter (mm)	Pin Length (mm)	Shoulder Diameter (mm)	Pin Profile	Shoulder Future	Heat Treatment
H13 steel	5.0	3.0	12.0	Threaded	Flat	52–56 HRC

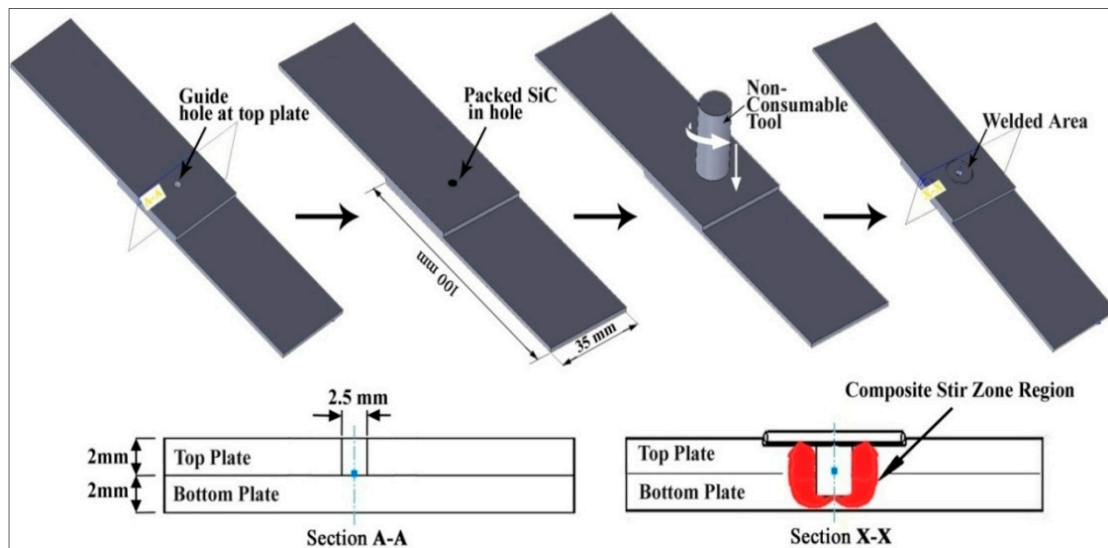


Figure 2. Sequence of the steps of the FSSW process adopted in the present research.

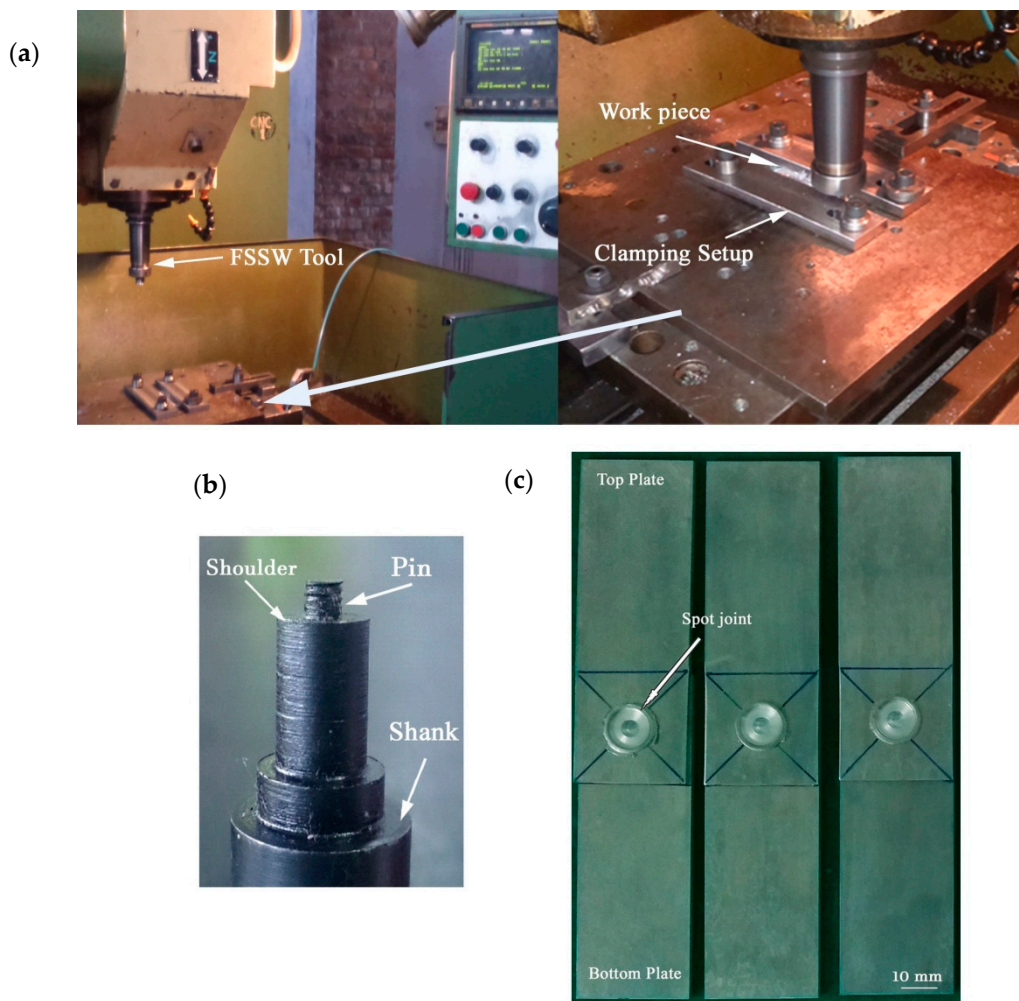
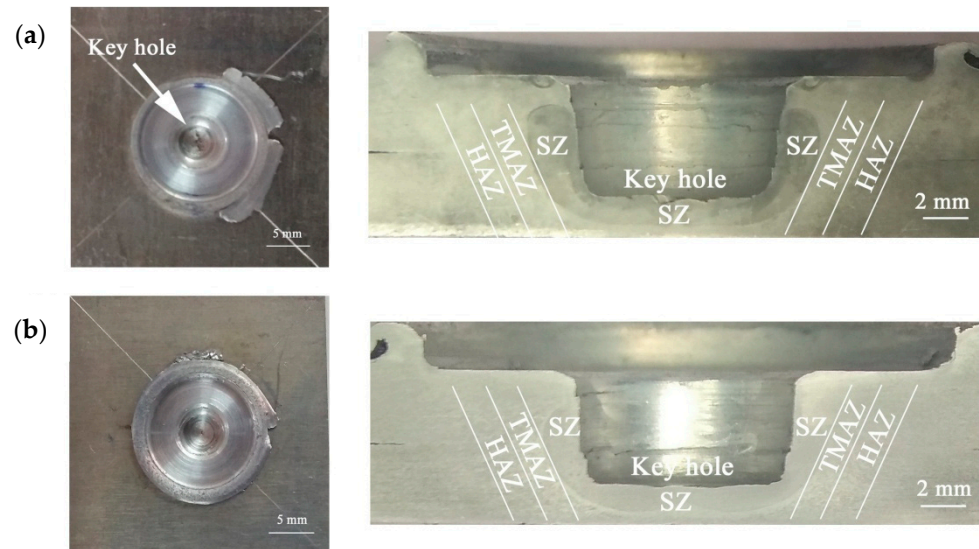


Figure 3. (a) FSSW setup. (b) FSSW tool used for the experiments. (c) Fabricated spot-weld joints.

### 2.1. Macroscopic View of the Composite Joints

Neither the AA5083/nano-SiC weld joints nor the AA5083/micro-SiC composite weld joints exhibited any remarkable defects or voids. Figure 4a shows the typical crown appearance and a cross-section of the AA5083/nano-SiC weld joints. Figure 4b shows the same for the AA5083/micro-SiC composite weld joints. The crowns appeared to be smooth, with no depressions or prominences, and the cross-sections had no internal defects. Therefore, it was confirmed that selected welding process parameters were adequate for producing defect-free joints.



**Figure 4.** Crown appearances and cross-sectional views of the FSSW joints: (a) AA5083/nano-SiC, and (b) AA5083/micro-SiC.

### 2.2. Mechanical and Tribological Characteristics

To explore the mechanical characterization of the fabricated AA5083 composite joints, lap shear tensile tests, microhardness tests, and wear tests were conducted. The tensile shear test specimens were prepared in accordance with ASTM E8-M03 [34]. The lap shear tensile tests were performed using a universal testing machine (TE-JINAN-WDW100) equipped with a load cell of 100 kN, and each sample was tested at room temperature at a crosshead speed of 1 mm/min.

The microhardness tests were performed on various weld zones of a cross-sectioned specimen using Vicker's hardness tester (Wilson Hardness-402 MVD). They were completed using 1 kg of force and 20 s of dwell time.

The dry sliding wear tests were performed at room temperature, as per the ASTM G99 [38] standard, using a pin-on-disc wear test device (Ducom TR20). For the wear tests, the specimens extracted from the stir zone (SZ) of the cross-sectioned welded samples were used. The test conditions were 20 N normal load, 2 m/s sliding speed, and 1000 m sliding distance.

### 2.3. X-ray Diffraction (XRD) and Microscopic Studies

The microstructures of the samples etched with Barker's reagent were observed using an optical microscope (Invertoplan TR, Gippon-Japan) and a field emission scanning electron microscope (FEDEM: AIGMA HV-Carl Zeiss, Germany). X-ray diffraction (XRD: X'Pert<sup>3</sup> Powder) was used to evaluate the formation of the phases in the stir zones.

### 3. Results and Discussion

#### 3.1. Microscopic Characterization of the Welds

The cross-sectional macroscopic appearances and the microscopic structures of the different zones in the AA5083/nano-SiC weld joints and the AA5083/micro-SiC weld joints are shown in Figures 5 and 6, respectively. The SZ of both the nano- and micro-SiC reinforced joints showed recrystallized equiaxed small grains, which were attributed to the thermo-mechanical process. Remarkably, the grains in the SZ of the nano-SiC-added weld joints were finer compared to the micro-SiC-added weld joints [39].

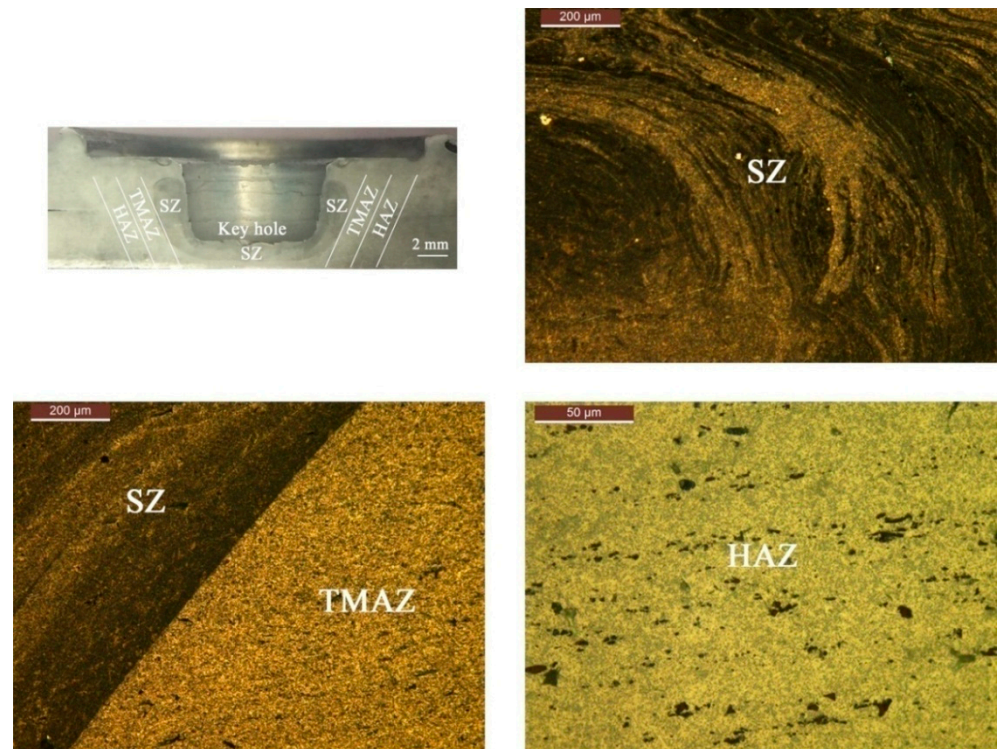


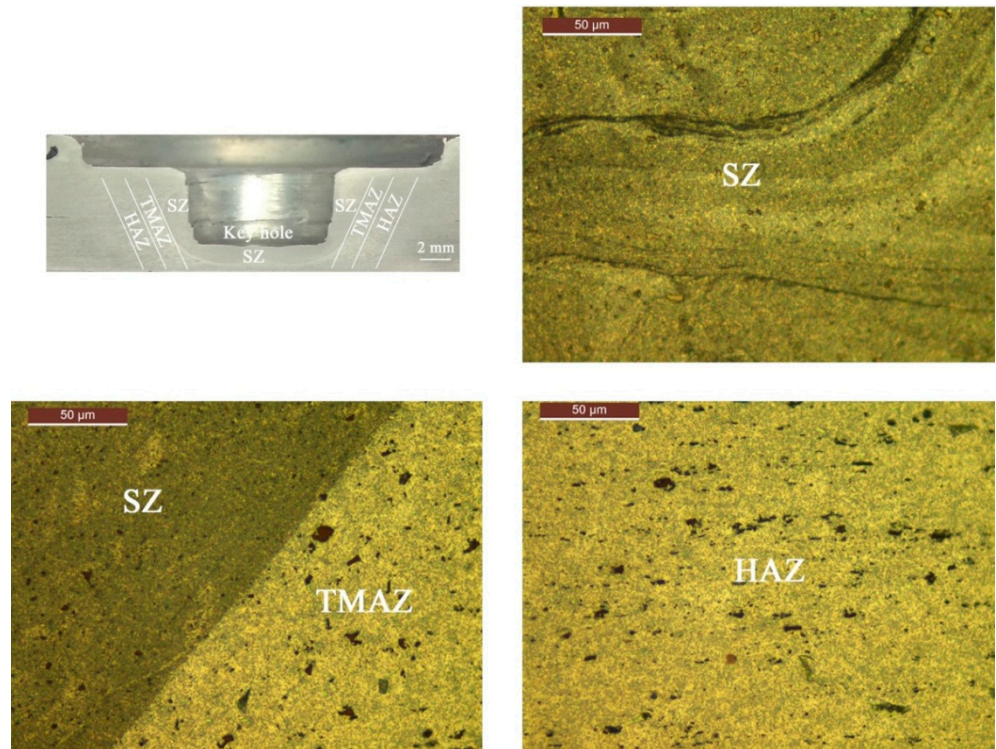
**Figure 5.** Optical micrographic views showing the various zones (SZ, TMAZ, and HAZ) of the AA5083/nano-SiC joints.

The finer grains of the nano-SiC-added weld could help in the formation of finer recrystallized equiaxed grains in the SZ. The grain refinement was caused by the pinning effect of the SiC particles, which impeded the grain growth by suppressing grain boundary sliding [40]. Further, the thermo-mechanically affected zones (TMAZ) of both composite joints had finer grains. The grain morphology in the heat-affected zone (HAZ) resembled that of the corresponding base material (BM).

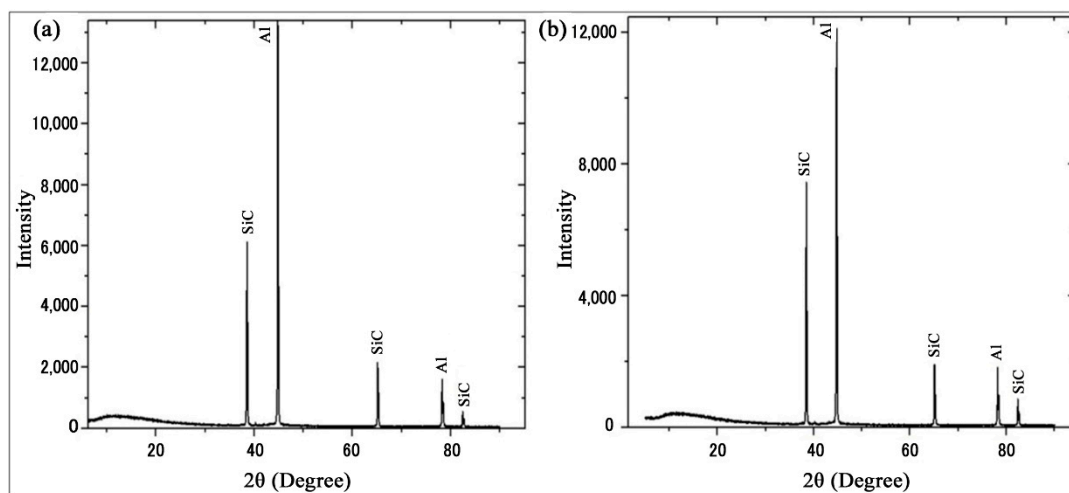
The XRD patterns of the micro- and nano-sized SiC-particle-reinforced FSSW joints are shown in Figure 7. The peaks of SiC in both the micro- and nano-composite FSSW joints appeared weak because the volume fraction of the SiC was smaller than of the substrate material (Al). Figure 7 also shows that there was no evidence of a new phase (intermetallic compounds). This could be attributed to the adequate heat generated during the FSSW. Moreover, some SiC reflections disappeared because of the good dispersion and size reduction of the fillers.

Figure 8 shows the FESEM micrographs in center of the SZs of both of the joint types. Within the SZs, the reinforced particles were distributed quite homogeneously. The nano-SiC-reinforced FSSW joints showed the finest particle distribution at the SZ compared to that of the micro-SiC-reinforced FSSW joints (Figure 8a). The SZ of the nano-SiC-reinforced FSSW joints had a homogeneous distribution of the particles and moderately dispersed particle regions. However, the micro-SiC-reinforced FSSW joints had agglomerations of

particles, regions with moderately dispersed particles, and particle-free regions, as shown in Figure 8b. Due to fragmentation occurring in the SZs, many clusters could be broken up into small particles and agglomerated, and some clusters could be distributed uniformly in the SZs due to the severe plastic deformation that occurred during the FSSW [41].



**Figure 6.** Optical micrographic views showing the various zones (SZ, TMAZ, and HAZ) of the AA5083/micro-SiC joints.



**Figure 7.** XRD pattern of FSSW joints: (a) AA5083/nano-SiC, and (b) AA5083/micro-SiC.



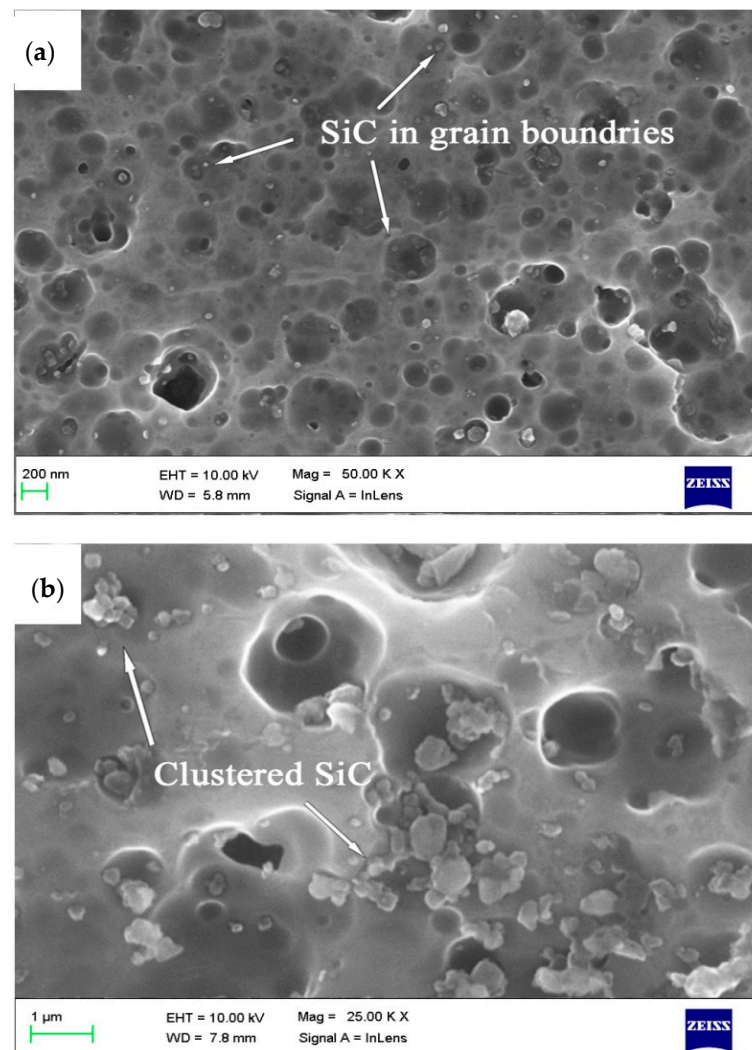


**Figure 8.** FESEM images of the SZs of the FSSW joints: (a) AA5083/nano-SiC, and (b) AA5083/micro-SiC.

However, it was observed that the particle-free regions in the SZs of AA5083/micro-SiC joints were larger than those of the AA5083/nano-SiC joints. Particle fragmentation occurred during the FSSW processes for both the nano- and micro-SiC additions; however, because of the relatively smaller size of the reinforced particles, it was considered to be less significant.

### 3.2. Lap Shear Strength

Figure 9a shows the lap shear fracture load of an AA5083 sample (with no filler), an AA5083/micro-SiC joint, and an AA5083/nano-SiC FSSW joint, while Figure 9b–d depicts their corresponding load-displacement curves. The lap shear fracture loads of the AA5083/micro-SiC and AA5083/nano-SiC FSSW joints were 3440 N and 4298 N, respectively, while that of the AA5083 sample (with no filler) was 3023 N. It is evident that the incorporation of SiC enhanced the lap shear strength of the joints, and in particular, the nano-SiC particles gave rise to a 29.6% higher strength. Particle agglomeration in the SZs may have been the reason for the lower lap shear strength in the micro-SiC-added joints. The nano-SiC-added joints had the highest lap shear strength because of the uniformly dispersed nanoparticles in the welded areas caused by the friction stir process. Adding to this, the decrease in grain size may have strengthened the grain boundaries and prevented grain growth at the grain boundaries [42,43]. This is evidenced in Figure 8a.

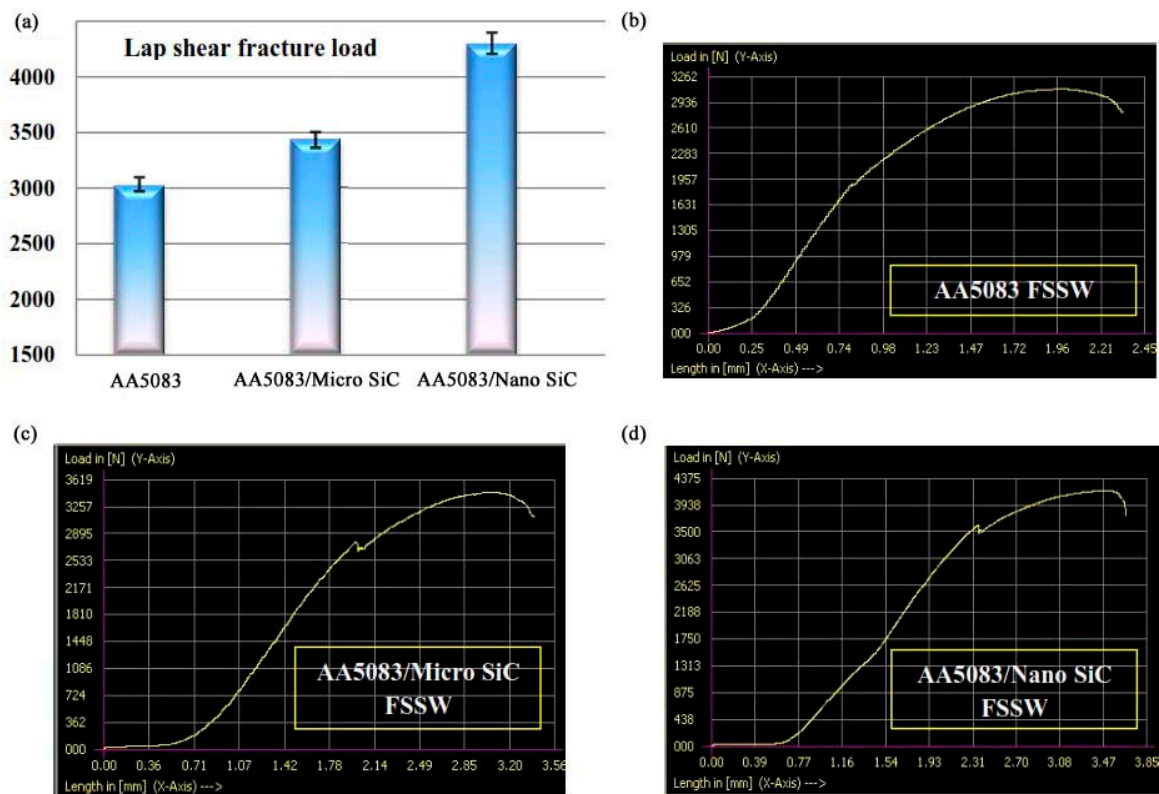


**Figure 9.** (a) Lap shear fracture load. (b–d) Load–displacement curves.

As shown in Figure 9b–d, it was found that the specimens made with the addition of particles showed significant increases in elongation compared to the specimens made without the addition of particles, as evidenced by the ductile behavior of the joints. These results are in consensus with the findings of Wu et al. [32] and Singh et al. [44].

### 3.3. Microhardness

Microhardness was measured 1 mm below the interface of the top and bottom plates of the AA5083 samples welded by FSSW. To test the microhardness, equal distances from the weld centers were maintained. Figure 10 shows the average microhardness values in the respective zones of the AA5083/micro-SiC and AA5083/nano-SiC FSSW joints. Without the addition of the nanoparticles, the samples welded by FSSW exhibited low microhardness values in the SZs. The SiC-particle-added SZs had re-precipitation compared to the particle-free SZs.

The uniformly dispersed fine SiC particles (both the nano- and micro-SiC) in the processed zones provided more nucleation sites for the re-precipitation of new grains and more precipitates in the aluminum matrix. The AA5083/nano-SiC samples showed the highest microhardness values ( $107 \pm 2$  HV) compared to the AA5083/micro-SiC samples ( $94.7 \pm 2$  HV). The increase in the SZ's microhardness compared to that of the other zones was due to the grain size reduction in this region (Hall–Petch relation) [30,45]. The nano-sized particles led to the formation of grain growth, which minimized the microhardness values in the SZs. Further, we perceived that the addition of the SiC particles did not significantly influence the TMAZs and the HAZs.

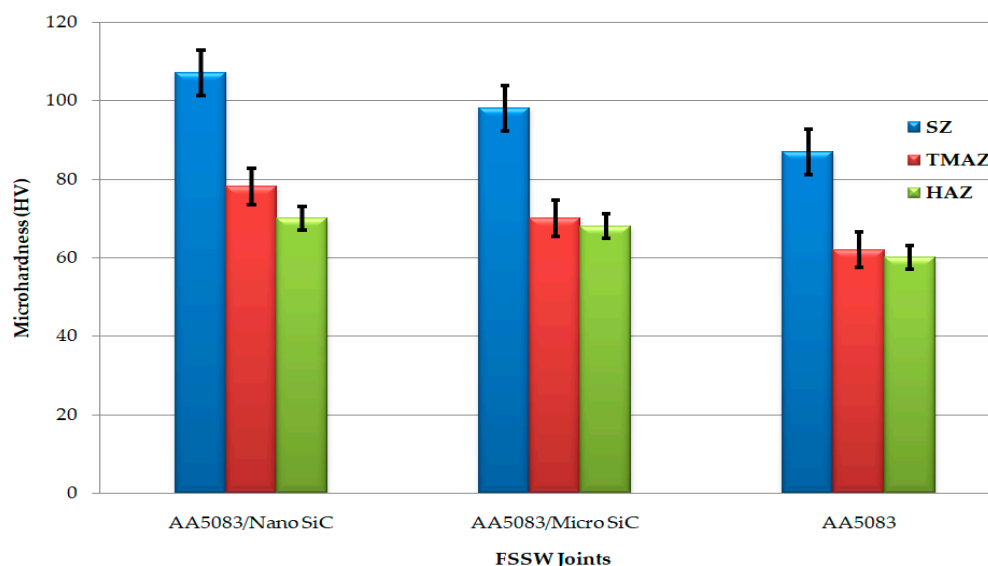


**Figure 10.** Microhardness measured transversely along different zones (SZs, TMAZs, and HAZs) for the FSSW SiC-particle-reinforced AA5083 samples and the without-reinforcement AA5083 samples.

### 3.4. Wear Behavior

Table 3 shows the variations in the coefficients of friction and wear ( $\mu\text{m}$ ) among the different FSSW joints. It was observable that particle-added joints had better wear resistance in comparison to particle-free joints. The significant reduction in wear was the result of the good dispersion of the SiC particles and the fine grain structures as compared to the particle-free joints. It is commonly known that enhancement of the hardness of a material increases its wear resistance [46]. Furthermore, the load-bearing characteristics of the hard SiC particles are the cause of this reduction in the contact stress between the joints and discs used in the tests [47]. Figure 11 shows a coefficient of friction plot for the running period of 950 s. It can be seen that the coefficient of friction of the SiC-added FSSW was considerably higher than that of the SiC-free specimen. This is because the hard SiC particles in the composite functioned as barriers, resulting in increased resistance to the surface [28,48,49]. The coefficient of friction of the nano-SiC-added weld joints was higher (0.345) than that of the specimen with micro-sized particles (0.301).

Figure 12 shows the FESEM images of the worn surfaces of the FSSW samples. The morphologies of the test surfaces show significant differences among the samples. The samples without the addition of SiC exhibited severe plastic deformation and surface layer removal compared to the SiC-added joints. Among all the welded samples, the nano-SiC-added sample underwent the least wear and showed shallow pits, as evidenced in Figure 12b. The presence of agglomerated micro-SiC particles was the reason for the higher number of pits in the micro-SiC-added joints, as evidenced in Figure 12c.

**Table 3.** Wear behaviors of the SFSSW joints with and without the addition of SiC particles.

Weld Joint	Wear ( $\mu\text{m}$ )	Coefficient of Friction
AA5083/nano-SiC	187	0.345
AA5083/micro-SiC	213	0.301
AA5083	254	0.283

With the understanding that nano-SiC-reinforced AA5083-H116 joints have higher weld strength than AA5083-H116-only joints, this research methodology can be extended to other materials. In recent years, there has been increased research interest in fabricating polymer joints through the FSW/FSSW processes [50–52]. Pereira et al. [50] and Ramesh Rudrapati [51] reported in their reviews that further investigations and research are required

to find the appropriate plunge force, temperature, fiber fragmentation degree, tilt angle, tool geometry, and rotational speed for conducting FSW on polymer composites. Jalal Joudaki et al. [52] successfully demonstrated the FSW of polymer-AA 1050 (PTFE-Al) composites. Innovations in the current method for fabricating composite FSSW joints provides an ideal framework for fabricating reinforced polymer/polymer matrix composite spot joints to reduce costs and improve productivity, with low environmental impacts, in the aerospace, automobile, and electronic device industries.

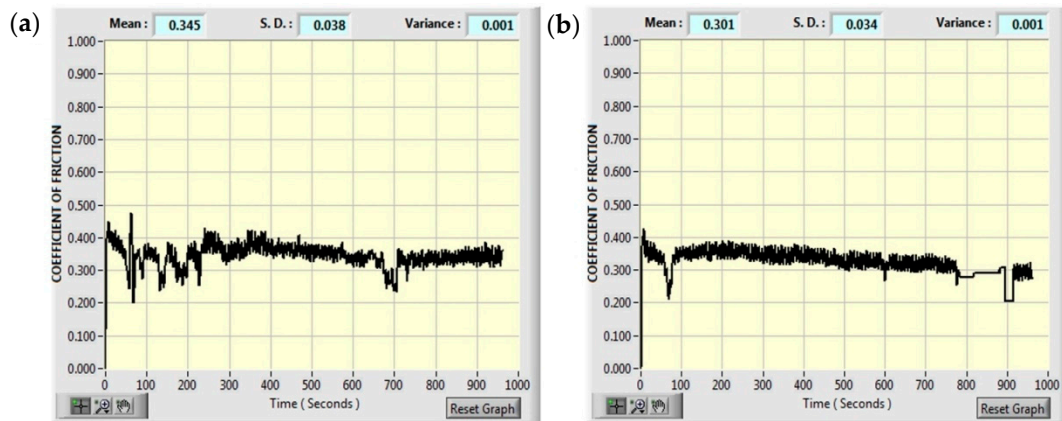


Figure 11. Evolution of the coefficients of friction: (a) AA5083/nano-SiC, and (b) AA5083/micro-SiC.

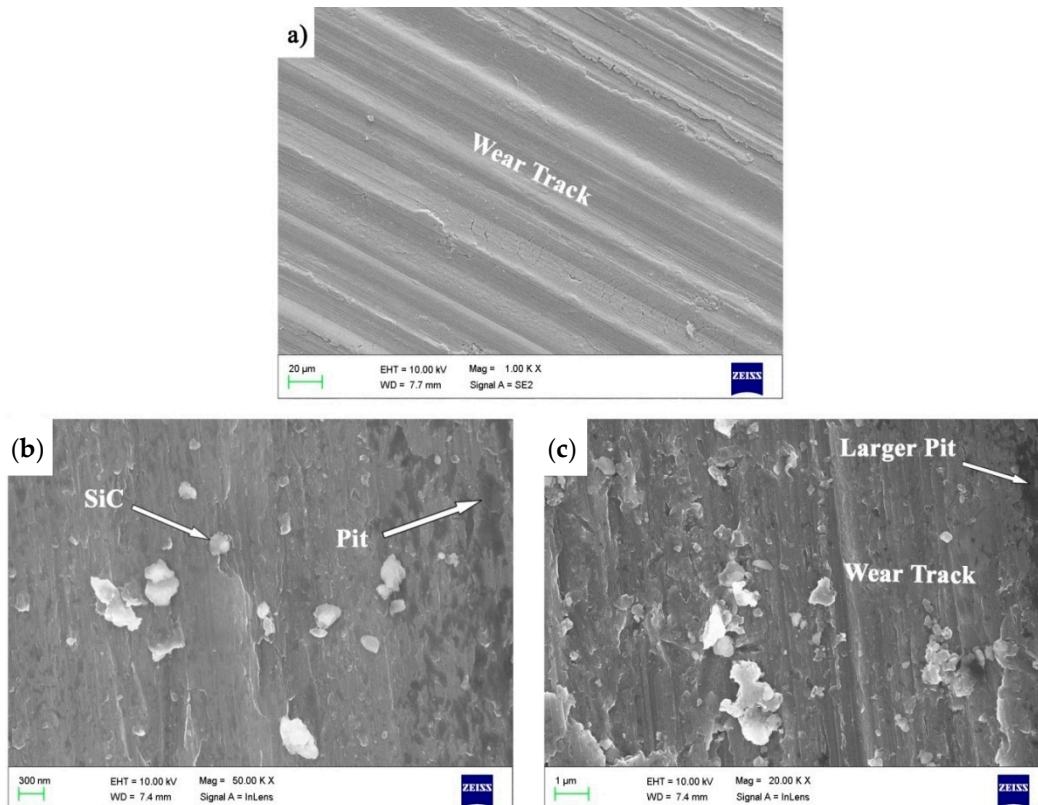


Figure 12. FESEM micrographs of the worn surfaces of the FSSW joints: (a) AA5058, (b) AA5083/nano-SiC, and (c) AA5083/micro-SiC.

#### 4. Conclusions

From the research conducted on the friction stir spot-welding of AA5083-H116 with micro- and nano-SiC particles, the following conclusions can be drawn:

- The addition of micro- and nano-SiC particles into spot joints improves both the mechanical and tribological properties of the joints.
- The addition of nano-SiC particles, in particular, increases lap shear strength by 29.3%, hardness by 23.3%, and wear property by 26.3%.
- The superior material flow of the nano-SiC particles in the SZs improved the mixing of the aluminum/SiC particles, and a more homogenized SZ was the result. Some agglomerations of particles were seen in the micro-SiC-particle-added joints that consequently reduced their mechanical and tribological properties compared to those of the nano-SiC-added joints. The improvement in the hardness, tensile strength, and wear resistance of the FSSW joints was the result of the grain refinement and uniform dispersion of the reinforcement particles.

**Author Contributions:** Conceptualization, E.N. and G.F.; methodology, S.R.; software, S.S.; validation, S.S. and E.N.; formal analysis, S.S.; investigation, S.S.; resources, E.N.; data curation, S.S.; writing—original draft preparation, S.S.; writing—review and editing, E.N. and G.F.; visualization, S.R.; supervision, E.N.; project administration, S.S. All authors have read and agreed to the published version of the manuscript.

**Funding:** This research received no external funding.

**Institutional Review Board Statement:** Not Applicable.

**Informed Consent Statement:** Not Applicable.

**Data Availability Statement:** Not applicable.

**Conflicts of Interest:** The authors declare no conflict of interest. The funders had no role in the design of the study; in the collection, analyses, or interpretation of data; in the writing of the manuscript; or in the decision to publish the results.

## References

1. Chen, R.-Y.; Chu, H.-Y.; Lai, C.-C.; Wu, C.-T. Effects of annealing temperature on the mechanical properties and sensitization of 5083-H116 aluminum alloy. *Proc. Inst. Mech. Eng. Part L J. Mater. Des. Appl.* **2015**, *229*, 339–346. [[CrossRef](#)]
2. Summers, P.T.; Chen, Y.; Rippe, C.M.; Allen, B.; Mouritz, A.P.; Case, S.W.; Lattimer, B.Y. Overview of aluminum alloy mechanical properties during and after fires. *Fire Sci. Rev.* **2015**, *4*, 3. [[CrossRef](#)]
3. Kala, H.; Mer, K.K.S.; Kumar, S. A review on mechanical and tribological behaviors of stir cast aluminum matrix composites. *Procedia Mater. Sci.* **2014**, *6*, 1951–1960. [[CrossRef](#)]
4. Neelamegam, V.; Govindasamy Bhavani, B.; Muthukrishnan, M.; Tadivaka, S.R. Investigation on corrosion behavior of cryogenically treated friction stir welded AA5083. *Mechanika* **2020**, *26*, 442–449. [[CrossRef](#)]
5. Kah, P.; Rajan, R.; Martikainen, J.; Suoranta, R. Investigation of weld defects in friction-stir welding and fusion welding of aluminium alloys. *Int. J. Mech. Mater. Eng.* **2015**, *10*, 26. [[CrossRef](#)]
6. Shen, Z.; Ding, Y.; Gerlich, A.P. Advances in friction stir spot welding. *Crit. Rev. Solid State Mater. Sci.* **2020**, *45*, 457–534. [[CrossRef](#)]
7. Suresh, S.; Venkatesan, K.; Rajesh, S. Optimization of process parameters for friction stir spot welding of AA6061/Al<sub>2</sub>O<sub>3</sub> by Taguchi method. *AIP Conf. Proc.* **2019**, *2128*, 030018. [[CrossRef](#)]
8. Yang, X.W.; Fu, T.; Li, W.Y. Friction stir spot welding: A review on joint macro- and microstructure, property, and process modelling. *Adv. Mater. Sci. Eng.* **2014**, *2014*, 697170. [[CrossRef](#)]
9. Heidarzadeh, A.; Mironov, S.; Kaibyshev, R.; Çam, G.; Simard, A.; Gerlich, A.; Khodabakhshi, F.; Mostafaei, A.; Field, D.P.; Robson, J.D.; et al. Friction stir welding/processing of metals and alloys: A comprehensive review on microstructural evolution. *Prog. Mater. Sci.* **2021**, *117*, 100752. [[CrossRef](#)]
10. Anton Savio Lewise, K.; Edwin Raja Dhas, J. FSSW process parameter optimization for AA2024 and AA7075 alloy. *Mater. Manuf. Process.* **2021**, *37*, 34–42. [[CrossRef](#)]
11. Manickam, S.; Rajendran, C.; Balasubramanian, V. Investigation of FSSW parameters on shear fracture load of AA6061 and copper alloy joints. *Heliyon* **2020**, *6*, e04077. [[CrossRef](#)] [[PubMed](#)]
12. Bagheri, B.; MahdianRizi, A.A.; Abbasi, M.; Givi, M. Friction stir spot vibration welding: Improving the microstructure and mechanical properties of Al5083 joint. *Metallogr. Microstruct. Anal.* **2019**, *8*, 713–725. [[CrossRef](#)]
13. Kalaf, O.; Nasir, T.; Asmael, M.; Safaei, B.; Zeeshan, Q.; Motallebzadeh, A.; Hussain, G. Friction stir spot welding of AA5052 with additional carbon fiber-reinforced polymer composite interlayer. *Nanotechnol. Rev.* **2021**, *10*, 201–209. [[CrossRef](#)]
14. Bagheri, B.; Shamsipur, A.; Abdollahzadeh, A.; Mirsalehi, S.E. Investigation of SiC nanoparticle size and distribution effects on microstructure and mechanical properties of Al/SiC/Cu composite during the FSSW process: Experimental and simulation. *Met. Mater. Int.* **2022**. [[CrossRef](#)]

15. Akinlabi, E.T.; Ikumapayi, O.M.; Osinubi, A.S.; Madushele, N.; Abegunde, O.O.; Fatoba, S.O.; Akinlabi, S.A. Characterizations of AA5083-H116 produced by friction stir spot welding technique. *Adv. Mater. Process. Technol.* **2022**. [[CrossRef](#)]
16. Hassanifard, S.; Ghiasvand, A.; Varvani-Farahani, A. Fatigue response of aluminum 7075-T6 joints through inclusion of Al<sub>2</sub>O<sub>3</sub> particles to the weld nugget zone during friction stir spot welding. *J. Mater. Eng. Perform.* **2022**, *31*, 1781–1790. [[CrossRef](#)]
17. Janga, V.S.R.; Awang, M. Influence of plunge depth on temperatures and material flow behavior in refill friction stir spot welding of thin AA7075-T6 sheets: A numerical study. *Metals* **2022**, *12*, 927. [[CrossRef](#)]
18. Tiwan, H.; Ilman, M.N.; Kusmono, K. Effect of pin geometry and tool rotational speed on microstructure and mechanical properties of friction stir spot welded joints in AA2024-O aluminum alloy. *Int. J. Eng.* **2021**, *34*, 1949–1960. [[CrossRef](#)]
19. Karthikeyan, R. Establishing relationship between optimised friction stir spot welding process parameters and strength of aluminium alloys. *Adv. Mater. Process. Technol.* **2021**, *8*, 1173–1195. [[CrossRef](#)]
20. Balamurugan, M.; Gopi, S.; Mohan, D.G. Influence of tool pin profiles on the filler added friction stir spot welded dissimilar aluminium alloy joints. *Mater. Res. Express* **2021**, *8*, 096531. [[CrossRef](#)]
21. Gao, Y.; Liang, Y.; Ren, X.; Paidar, M. Pre-hole friction stir spot welding (PFSSW) for dissimilar welding of AA2219 to AA3003 sheets. *Vacuum* **2020**, *182*, 109688. [[CrossRef](#)]
22. Suryanarayanan, R.; Sridhar, V.G. Effect of process parameters in pinless friction stir spot welding of Al5754-Al6061 alloys. *Metallogr. Microstruct. Anal.* **2020**, *9*, 261–272. [[CrossRef](#)]
23. Rohani Yazdi, S.; Beidokhti, B.; Haddad-Sabzevar, M. Pinless tool for FSSW of AA 6061-T6 aluminum alloy. *J. Mater. Process. Technol.* **2019**, *267*, 44–51. [[CrossRef](#)]
24. Suresh, S.; Venkatesan, K.; Natarajan, E.; Rajesh, S.; Lim, W.H. Evaluating weld properties of conventional and swept friction stir spot welded 6061-T6 aluminium alloy. *Mater. Express* **2019**, *9*, 851–860. [[CrossRef](#)]
25. Fahmy, M.H.; Abdel-Aleem, H.A.; El-kousy, M.R.; Abdel-Elraheem, N.M. Comparative study of spot welding and friction stir spot welding of Al 2024-T3. *Key Eng. Mater.* **2018**, *786*, 104–118. [[CrossRef](#)]
26. Sun, Y.; Morisada, Y.; Fujii, H.; Tsuji, N. Ultrafine grained structure and improved mechanical properties of low temperature friction stir spot welded 6061-T6 Al alloys. *Mater. Charact.* **2018**, *135*, 124–133. [[CrossRef](#)]
27. Selvam, J.D.R.; Dinaharan, I.; Rai, R.S. Matrix and reinforcement materials for metal matrix composites. *Encycl. Mater. Compos.* **2021**, *2*, 615–639. [[CrossRef](#)]
28. Casati, R.; Vedani, M. Metal matrix composites reinforced by nano-particles—A review. *Metals* **2014**, *4*, 65–83. [[CrossRef](#)]
29. Sachinkumar; Narendranath, S.; Chakradhar, D. Microstructure, hardness and tensile properties of friction stir welded aluminum matrix composite reinforced with SiC and fly ash. *Silicon* **2019**, *11*, 2557–2565. [[CrossRef](#)]
30. Bhushan, R.K.; Sharma, D. Optimization of friction stir welding parameters to maximize hardness of AA6082/Si<sub>3</sub>N<sub>4</sub> and AA6082/SiC composites joints. *Silicon* **2021**, *14*, 643–661. [[CrossRef](#)]
31. Fereiduni, E.; Movahedi, M.; Baghdadchi, A. Ultrahigh-strength friction stir spot welds of aluminium alloy obtained by Fe<sub>3</sub>O<sub>4</sub> nanoparticles. *Sci. Technol. Weld. Join.* **2018**, *23*, 63–70. [[CrossRef](#)]
32. Wu, D.; Shen, J.; Lv, L.; Wen, L.; Xie, X. Effects of nano-SiC particles on the FSSW welded AZ31 magnesium alloy joints. *Mater. Sci. Technol.* **2017**, *33*, 998–1003. [[CrossRef](#)]
33. Tebyani, S.F.; Dehghani, K. Friction stir spot welding of interstitial free steel with incorporating silicon carbide nanopowders. *Int. J. Adv. Manuf. Technol.* **2015**, *79*, 343–350. [[CrossRef](#)]
34. Suresh, S.; Venkatesan, K.; Natarajan, E. Influence of SiC nanoparticle reinforcement on FSS welded 6061-T6 aluminum alloy. *J. Nanomater* **2018**, *2018*, 7031867. [[CrossRef](#)]
35. Hannachi, N.; Khalfallah, A.; Leitao, C.; Rodrigues, D.M. A comparative study on the physical and mechanical behavior of AA6082-T6 and AA5083-H116 aluminum alloys in friction stir spot welding. In *Advances in Mechanical Engineering, Materials and Mechanics. ICAMEM 2019. Lecture Notes in Mechanical Engineering*; Kharrat, M., Baccar, M., Dammak, F., Eds.; Springer: Cham, Switzerland, 2020. [[CrossRef](#)]
36. Akinlabi, E.T.; Osinubi, A.S.; Madushele, N.; Akinlabi, S.A.; Ikumapayi, O.M. Data on microhardness and structural analysis of friction stir spot welded lap joints of AA5083-H116. *Data Br.* **2020**, *33*, 106585. [[CrossRef](#)] [[PubMed](#)]
37. Chupradit, S.; Bokov, D.O.; Suksatan, W.; Landowski, M.; Fydrych, D.; Abdullah, M.E.; Derazkola, H.A. Pin angle thermal effects on friction stir welding of AA5058 aluminum alloy: CFD simulation and experimental validation. *Materials* **2021**, *14*, 7565. [[CrossRef](#)]
38. Suresh, S.; Elango, N.; Ragavanantham, S.; Venkatesan, K.; Saravanakumar, N.; AntoDilip, A. Strategized friction stir welded AA6061-T6/SiC composite lap joint suitable for sheet metal applications. *J. Mater. Res. Technol.* **2022**, *21*, 30–39. [[CrossRef](#)]
39. Moradi, M.M.; Jamshidi Aval, H.; Jamaati, R. Microstructure and mechanical properties in nano and microscale SiC-included dissimilar friction stir welding of AA6061-AA2024. *Mater. Sci. Technol.* **2017**, *34*, 388–401. [[CrossRef](#)]
40. Liu, T.-S.; Qiu, F.; Dong, B.-X.; Geng, R.; Zha, M.; Yang, H.-Y.; Shu, S.-L.; Jiang, Q.-C. Role of trace nanoparticles in establishing fully optimized microstructure configuration of cold-rolled Al alloy. *Mater. Des.* **2021**, *206*, 109743. [[CrossRef](#)]
41. Raja, S.; Muhamad, M.R.; Jamaludin, M.F.; Yusof, F. A review on nanomaterials reinforcement in friction stir welding. *J. Mater. Res. Technol.* **2020**, *9*, 16459–16487. [[CrossRef](#)]
42. Suresh, S.; Venkatesan, K.; Natarajan, E.; Rajesh, S. Influence of tool rotational speed on the properties of friction stir spot welded AA7075-T6/Al<sub>2</sub>O<sub>3</sub> composite joint. *Mater. Today Proc.* **2020**, *27*, 62–67. [[CrossRef](#)]

43. Abioye, T.E.; Zuhailawati, H.; Anasyida, A.S.; Yahaya, S.A.; Dhindaw, B.K. Investigation of the microstructure, mechanical and wear properties of AA6061-T6 friction stir weldments with different particulate reinforcements addition. *J. Mater. Res. Technol.* **2019**, *8*, 3917–3928. [[CrossRef](#)]
44. Singh, T.; Tiwari, S.K.; Shukla, D.K. Mechanical and microstructural characterization of friction stir welded AA6061-T6 joints reinforced with nano-sized particles. *Mater. Charact.* **2020**, *159*, 110047. [[CrossRef](#)]
45. Suresh, S.; Venkatesan, K.; Natarajan, E.; Rajesh, S. Performance analysis of nano silicon carbide reinforced swept friction stir spot weld joint in AA6061-T6 alloy. *Silicon* **2021**, *13*, 3399–3412. [[CrossRef](#)]
46. Barmouz, M.; Asadi, P.; Besharati Givi, M.K.; Taherishargh, M. Investigation of mechanical properties of Cu/SiC composite fabricated by FSP: Effect of SiC particles' size and volume fraction. *Mater. Sci. Eng. A* **2011**, *528*, 1740–1749. [[CrossRef](#)]
47. Suresh, S.; Elango, N.; Venkatesan, K.; Lim, W.H.; Palanikumar, K.; Rajesh, S. Sustainable friction stir spot welding of 6061-T6 aluminium alloy using improved non-dominated sorting teaching learning algorithm. *J. Mater. Res. Technol.* **2020**, *9*, 11650–11674. [[CrossRef](#)]
48. Sudhagar, S.; Gopal, P.M. Investigation on mechanical and tribological characteristics Cu/Si<sub>3</sub>N<sub>4</sub> surface composite developed through friction stir processing. *Silicon* **2022**, *14*, 4207–4216. [[CrossRef](#)]
49. Suresh, S.; Natarajan, E.; Vinayagamurthi, P.; Venkatesan, K.; Viswanathan, R.; Rajesh, S. Optimum Tool Traverse Speed Resulting Equiaxed Recrystallized Grains and High Mechanical Strength at Swept Friction Stir Spot Welded AA7075-T6 Lap Joints. In *Materials, Design and Manufacturing for Sustainable Environment*; Lecture Notes in Mechanical Engineering; Natarajan, E., Vinodh, S., Rajkumar, V., Eds.; Springer: Singapore, 2022. [[CrossRef](#)]
50. Pereira, M.A.R.; Galvão, I.; Costa, J.D.; Amaro, A.M.; Leal, R.M. Joining of Fibre-Reinforced Thermoplastic Polymer Composites by Friction Stir Welding—A Review. *Appl. Sci.* **2022**, *12*, 2744. [[CrossRef](#)]
51. Ramesh Rudrapati. Effects of welding process conditions on friction stir welding of polymer composites: A review. *Compos. Part C Open Access* **2022**, *8*, 100269. [[CrossRef](#)]
52. Joudaki, J.; Safari, M.; Joudaki, M. Experimental investigation of friction stir spot welding of polymer-aluminum alloy weldments. *Proc. Inst. Mech. Eng. Part B J. Eng. Manuf.* **2022**, *236*, 1368–1379. [[CrossRef](#)]